Database-Assisted Wind Load Capacity Estimates for Low-Rise Steel Frames

Seokkwon Jang[1]; Le-Wu Lu, M.ASCE[2]; Fahim Sadek, M.ASCE[3]; and Emil Simiu, F.ASCE[4]

Abstract: A comparative study is presented of the estimated wind load capacities of low-rise steel building frames based on loading patterns (magnitude and distribution) established from aerodynamic databases on the one hand, and on patterns specified in the ASCE 7 Standard on the other. The estimated capacities are based on the assumption, verified by numerous sets of calculations, and also used in the development of the ASCE 7 Standard, that the most unfavorable wind load occurs at the instant in time when the peak knee-joint bending moment is attained. The estimates are obtained from detailed inelastic finite element analyses of the frames with ultimate states associated with local and global instabilities. It is shown that the estimates based on the aerodynamic database are more realistic and risk consistent and can therefore lead to safer designs at lower costs. These estimates represent a significant advance over the ASCE 7 Standard-based estimates.

DOI: 10.1061/(ASCE)0733-9445(2002)128:12(1594)

CE Database keywords: Building codes; Finite element method; Nonlinear analysis; Steel structures; Wind force; Reliability; Ultimate strength; Database.

Introduction

Wind loading provisions of the ASCE 7 Standard and its predecessors were developed to be simple enough for use with the slide rule or pocket calculator. For low-rise building frames, wind loads inherent in those provisions are independent of distance between frames (implying perfect lateral coherence of the wind loads), and are based on a generic set of the frames' influence lines, rather than on the actual influence lines. In addition, the ASCE 7 loads model the spatial variation of the actual wind loads in an oversimplified manner determined by the need to cover a wide variety of loading situations by a single table or diagram. For these reasons, calculations based on the ASCE 7 wind loads can result in (1) large differences between the Standard loads and the actual loads the Standard provisions are purported to mimic, and (2) significant inconsistencies with respect to risk. This is true for allowable stress design (ASD), strength design, and design based on nonlinear analyses yielding ultimate frame capacities.

In general, fluctuating wind loads acting on structures—especially low-rise buildings—cannot be described analytically, nor can they be calculated in sufficient detail using computational fluid dynamics. Rather, they must be obtained from measurements. Current wind tunnel measurement techniques make it possible to develop large aerodynamic databases consisting of simultaneous time histories of pressures obtained at large numbers of points on the building surface. The aerodynamic databases can be used for evaluating the risk consistency of ASCE 7 provisions for wind loads inducing linear structural behavior (Minciarelli et al. 2001a,b). The fluctuating wind load information yielded by the databases is also suitable for use in realistic calculations of nonlinear frame behavior, including local and global instabilities and plastic behavior.

This paper presents the initial results of such calculations. It has been possible to reproduce to within a close approximation the actual spatial variation of the external wind loads yielded by the aerodynamic databases. However, an accurate representation of the temporal variation of the wind loads has not been attempted. Rather, to define the wind loading for a particular frame and a particular wind direction, the time at which the time-dependent loading induces the peak value of the fluctuating bending moment at the controlling knee joint in the linearly elastic structure is observed. The time-invariant wind load is identical to the fluctuating wind load acting on the frame at that time. This approach was selected because it is consistent with the approach used in the development of the ASCE 7 Standard (see, e.g., Commentary to ASCE 7-95, p. 162). This allows a direct comparison between the aerodynamic databases and the Standard. The approach has been validated by extensive comparisons between the spatial configurations of the loads at various times. The comparisons showed that these configurations were approximately independent of time.

It is shown that ultimate frame capacities based on database-assisted load representations can differ significantly from ultimate capacities calculated on the basis of ASCE 7 loads. The study is focused on a low-rise steel building designed to be located near Miami, Fla. Simultaneous wind pressure time histories with a prototype duration of about 1 h were obtained from records of

[1]Graduate Student, Dept. of Civil and Environmental Engineering, Lehigh Univ., Bethlehem, PA 18015-3176.

[2]Professor, Dept. of Civil and Environmental Engineering, Lehigh Univ., Bethlehem, PA 18015-3176.

[3]Research Structural Engineer, Building and Fire Research Laboratory, National Institute of Standards and Technology, Gaithersburg, MD 20899-8611. E-mail: fahim.sadek@nist.gov

[4]NIST Fellow, Building and Fire Research Laboratory, National Institute of Standards and Technology, Gaithersburg, MD 20899-8611.

Note. Associate Editor: Bogusz Bienkiewicz. Discussion open until May 1, 2003. Separate discussions must be submitted for individual papers. To extend the closing date by one month, a written request must be filed with the ASCE Managing Editor. The manuscript for this paper was submitted for review and possible publication on April 19, 2001; approved on March 12, 2002. This paper is part of the ***Journal of Structural Engineering***, Vol. 128, No. 12, December 1, 2002. ©ASCE, ISSN 0733-9445/2002/12-1594–1603/$8.00+$.50 per page.

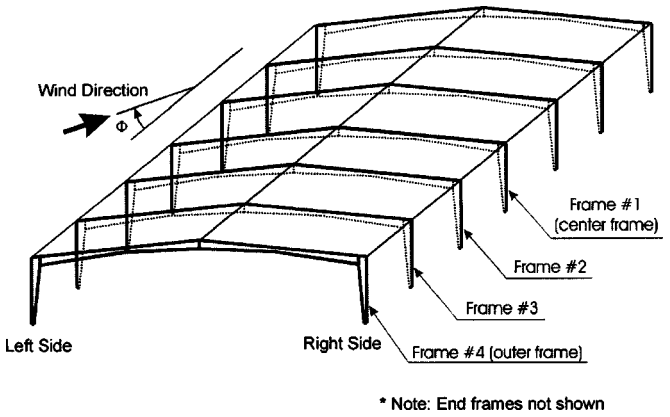

Fig. 1. Isometric view of interior frames

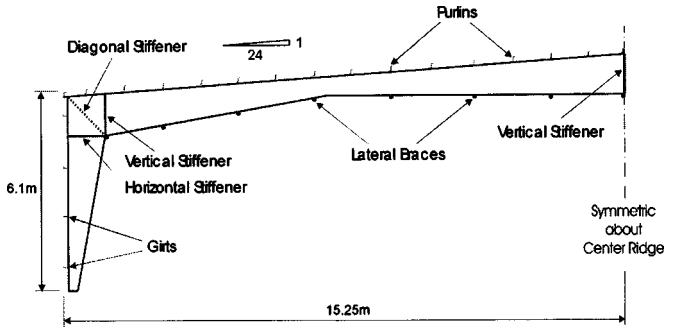

Fig. 2. Schematic diagram of typical frame

pressure time histories measured at the Univ. of Western Ontario on a wind tunnel model of the building (Lin and Surry, 1997).

Building, Frames, Aerodynamic Pressures, Wind Effects, and Load Combinations

Building Description

The building considered is assumed to be located in open terrain at 13 km inland near Miami. It is rectangular in plan with dimensions 61 m×30.5 m, 6.1 m eave height, gable roof with slope 1/24, and ridge parallel to the long building dimension. Its ASCE 7-93 Standard (1993) classification is Category 1.

For the direction normal to the ridge the main wind load-resisting system consists of two end frames and seven interior frames. The distance between interior frames is 7.62 m center to center. The end frames are equally spaced from the respective neighboring interior frame. An isometric view and designation of the frames (not including the end frames) are shown in Fig. 1.

Frame Designs, Details, and Nomenclature

The design of the frames was performed using the software developed by the Metal Building Manufacturers Association (MBMA), which is based on the ASCE 7-93 Standard (1993) and the AISC 1989 design manual (allowable stress design). Purlins are attached to the top flange of the rafters and girts are attached to the outer flanges of the columns.

The following features of lateral bracing and joint stiffening are considered:

1. (a) Lateral bracing to the bottom flanges of the rafters starting at the knee joint with a spacing of approximately 2.5 m. These braces restrain the rafters against lateral and torsional movements (Fig. 2); (b) alternatively, bottom lateral bracing with a spacing of about 6 m.
2. (a) Horizontal and vertical stiffeners at the knee joints; (b) alternatively, horizontal, vertical, and diagonal stiffeners at the knee joints.
3. A vertical stiffener is provided for the web of the rafter at the ridge in all cases.

The frames are designated by a sequence of letters as follows. The letter M indicates that the location of the building is Miami. (Future studies are planned for buildings in other locations.) The letter B indicates that the rafter's lower flanges have lateral bracing. The letters H or D indicate, respectively, that the knee joints have vertical and horizontal, or vertical, horizontal, and diagonal stiffeners. The letter R indicates that the distance between the rafter's lateral braces is approximately 6 m. The absence of the letter R indicates that distance is approximately 2.5 m.

Aerodynamic Pressure Coefficients

Aerodynamic pressures were measured by pressure taps, which were installed on a 1:200 wind tunnel model at about 440 locations as indicated in Fig. 3. The typical number of taps per unit area is about three to five times higher than that in the previous tests, the results of which were used in the development of the ASCE 7-93 provisions (see Fig. A1.1 in Davenport, Surry and Stathopoulos, 1977). Pressure-time histories were recorded for each of 37 wind directions between 0° and 180° at 5° intervals. Pressure coefficients C_p obtained from pressure measurements were referenced with respect to the experimental dynamic pressures at the eave height H. The wind tunnel mean hourly flow speed at the nominal gradient height (290 m for the prototype) was about 18.3 m/s, and the corresponding mean flow speed $V_h(H)$ at the model eave height was 10.15 m/s (Whalen et al. 1998). The characteristics of the wind tunnel flow conformed to the usual representation of the atmospheric boundary-layer flow over open terrain. The time series was sampled at 400 Hz for approximately 60 s. By virtue of the requirement that the reduced frequency nD/V (where n=characteristic frequency, D=characteristic length, and V=characteristic velocity) be the same for the model and the prototype, the sampling rate for the prototype is

$$n_p=[V_h(6.1\ \text{m})/10.15]400\ \text{Hz}/200\ \text{Hz} \tag{1}$$

For example, if $V_h(6.1\,\text{m})=36.94\,\text{m/s}$ (this corresponds to the ASCE 7-93 (1993) basic wind speed for Miami, as shown subsequently), then $n_p=7.28\,\text{Hz}$. The corresponding prototype record length is $T=60\,\text{s}\times 400/n_p=3{,}297\,\text{s}$, that is, approximately 1 h. For higher wind speeds the prototype record length is less than 1 h. However, this may be assumed to have a minor effect on the results being sought, especially if it is recalled that lengths of statistically stationary time series during the strongest winds associated with extreme storms rarely exceed 20 min or so. The processed time series were digitally low-pass filtered at 150 Hz. The resolution for the pressure coefficients was about 0.01.

Wind Effects

In keeping with the provisions of the ASCE 7-93 Standard (1993), which is used for frame design in the MBMA software mentioned earlier, the wind-induced pressures in N/m^2 are

J. Struct. Eng. 2002.128:1594-1603.

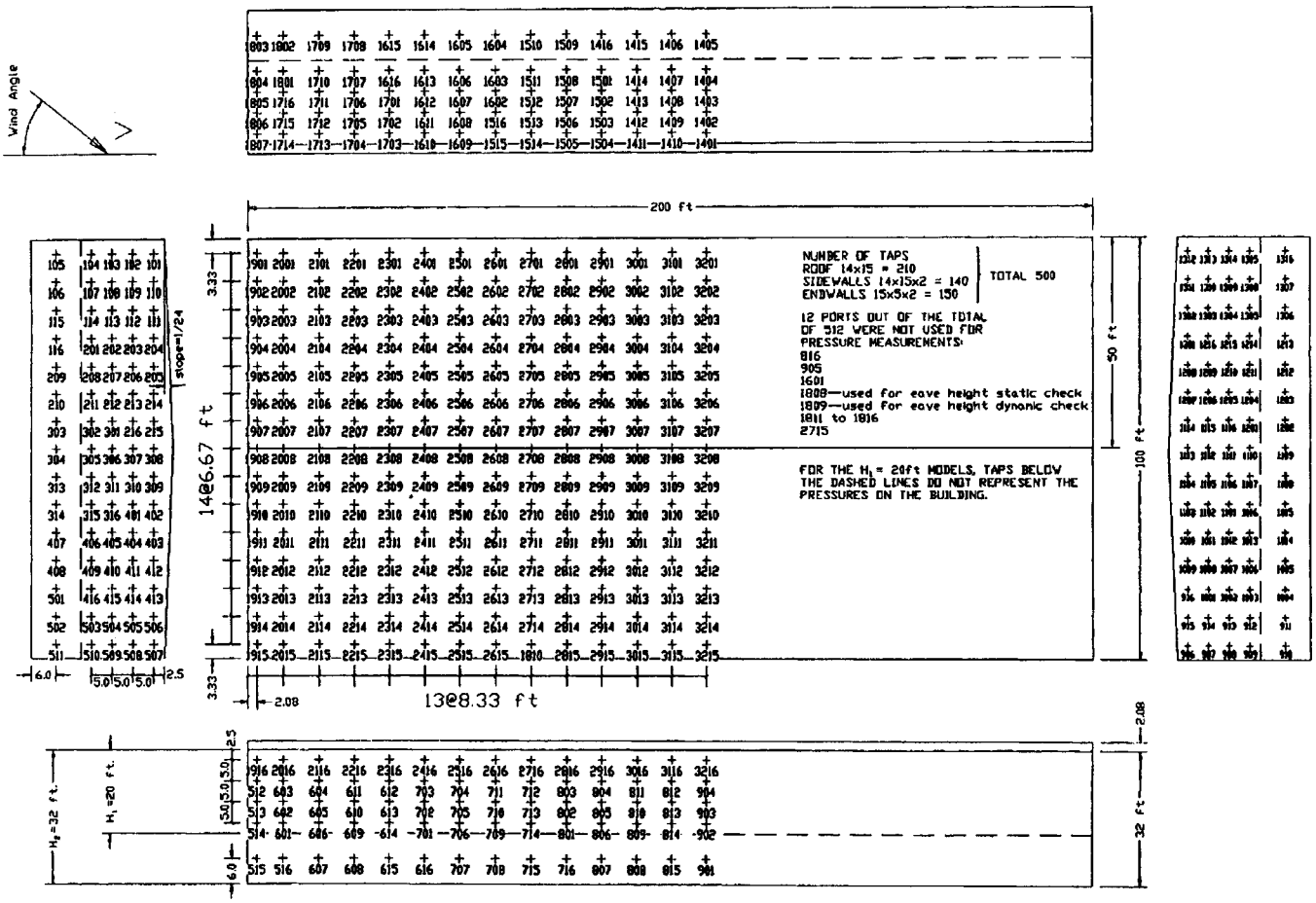

Fig. 3. Pressure taps arrangement (1 ft=0.3048 m. Figure taken from Lin and Surry 1997)

$$p(t) = 0.613 \; C_p(t) V_h^2(H) \tag{2}$$

$$V_h(H) = 1.046 (K_z)^{1/2} Vc \tag{3}$$

where C_p=pressure coefficient as determined from the wind tunnel tests, 1.046=importance factor for Category 1 buildings located at 13 km from the coastline [Table 5 of ASCE 7-93), H=eave height in m, $V_h(H)$=mean hourly speed in m/s at elevation H, V=fastest-mile wind speed in m/s at 10 m above ground in open terrain, $K_z=0.87$ is an exposure coefficient whose square root=a factor that transforms the fastest-mile wind speed at 10 m above ground in open terrain to the fastest-mile wind speed at elevation 6.1 m over open terrain [Table 6 of ASCE 7-93), and c=a factor that transforms fastest-mile wind speeds to mean hourly speeds [Sec. 6.5.2.2 and Fig. C5 of the Commentary to the ASCE 7-93 Standard (1993)]. The 50 year fastest-mile wind speed V specified in the ASCE 7-93 Standard (1993) for Miami is 49.6 m/s (111 mph). The factor c corresponds in Fig. C5 of ASCE 7-93 to the averaging time $t=(3{,}600/111)\text{s}=32\text{ s}$ (see also Simiu and Scanlan 1996). Therefore, $c=1/1.31$. To the 50 year fastest-mile wind speed at 10 m above ground in open terrain specified for Miami in ASCE 7-93, there corresponds the hourly mean speed at 6.1 m elevation (eave height) $V_h(6.1\text{ m})=1.046\times(0.87)^{1/2}\times 49.6/1.31=36.94\text{ m/s}$. If based on ASCE 7-98 Standard (1998) provisions $V_h(6.1\text{ m})$ in Eq. (3) it would be slightly larger (37.87 m/s).

The wind loads on a frame at the instant t were obtained by summing up the pressures at that instant at all taps contributing to the loading of the frame, times the respective tributary areas. Procedures are available for taking into account the combined directional effects of the extreme wind climate and aerodynamic pressures (see, e.g., Rigato et al. 2001). For consistency with the ASCE 7-93 provisions, however, the calculations are based on wind speeds estimated without regard for their direction, as in Eq. (3). The implications of the fact that the ASCE loads represent envelopes of measured loads multiplied by a blanket directionality reduction factor $k_d=0.85$ (Ellingwood et al. 1980) will be discussed later.

Load Combinations

Ultimate strength analyses were performed for the following seven load combination cases:

$$\text{Case 1: } \lambda(D+L_R); \quad \text{Case 2: } \lambda(D+W_S);$$

$$\text{Case 3: } \lambda(D+W_T);$$

$$\text{Case 4: } 1.2D+\lambda W_S+0.5L_R;$$

$$\text{Case 5: } 1.2D+\lambda W_T+0.5L_R;$$

$$\text{Case 6: } 0.9D+\lambda W_S; \quad \text{Case 7: } 0.9D+\lambda W_T$$

where D and L_R denote the ASCE 7-93 ASD dead load and roof live load, respectively. W_S denotes the wind load induced by a 50 year fastest-mile wind speed at 10 m above ground in open terrain, calculated in accordance with the ASCE 7-93 Standard (1993), which is the basis for the frames design by the MBMA software. The analyses also included W_S loads estimated using

J. Struct. Eng. 2002.128:1594-1603.

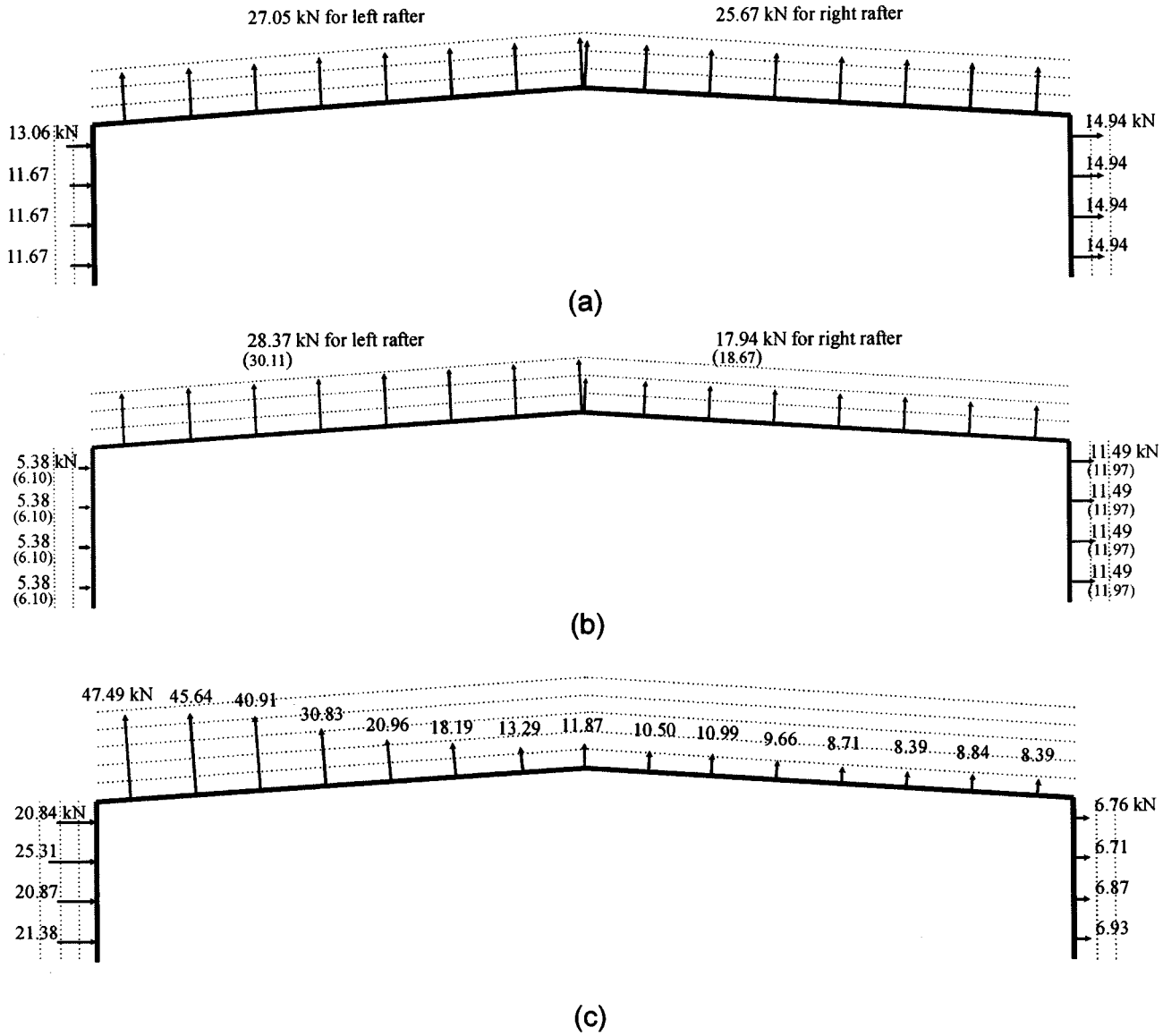

Fig. 4. (a) Wind forces W_S, specified by ASCE 7-93 Standard; (b) Wind forces W_S, specified by ASCE 7-98 Standard [( ) indicates wind forces W_S for frame 4]; and (c) wind forces W_T, obtained from aerodynamic database for frame 1, wind direction normal to ridge

the ASCE 7-98 provisions. W_T denotes the wind load induced by the same 50 year fastest-mile wind speed at 10 m above ground in open terrain, but calculated using Eqs. (1) and (2) and the recorded time series of the pressure coefficients obtained in the wind tunnel. For each load combination the factor λ that corresponds to failure through local and global instability effects was determined using a nonlinear finite element analysis program.

Definition of Wind Loading W_T

The calculations indicated that, with few exceptions of relatively minor significance, the controlling bending moment induced in the frame by the fluctuating wind loading occurs at the knee joints. For each load combination and each direction being considered, the time instant at which that knee bending moment was largest in the linearly elastic structure was determined. The simplifying assumption that the frame is subjected to a time-invariant external wind loading equal to the external wind loading acting on the frame at that time was then used. The assumed time-invariant load is, therefore, larger than the measured external fluctuating wind load at any other time. This procedure is consistent with the method used in the development of the ASCE 7 Standard and thus allows a direct comparison between the capacities computed using the aerodynamic databases and the standard. A more complete investigation could consider loadings corresponding to peak moments occurring at other cross sections such as the ridge or the rafter quarter span, to account for the few exceptions where the knee is not controlling.

In the absence of wind tunnel information on time-dependent internal pressures, the internal wind load specified in the ASCE 7-93 Standard (1993) was used in all the calculations. Tests currently being conducted at the Univ. of Western Ontario will provide a database on both external and internal pressure measurements. Future estimates of wind effects on frames will incorporate internal pressure measurements as well.

A sample case of the differences between the ASCE 7 loads and the assumed loads is shown in Fig. 4. The assumed load, W_T, pertains to the most unfavorable wind direction for frame 1 (wind parallel to the plane of the frame). Recall that W_T (i.e., the wind

J. Struct. Eng. 2002.128:1594-1603.

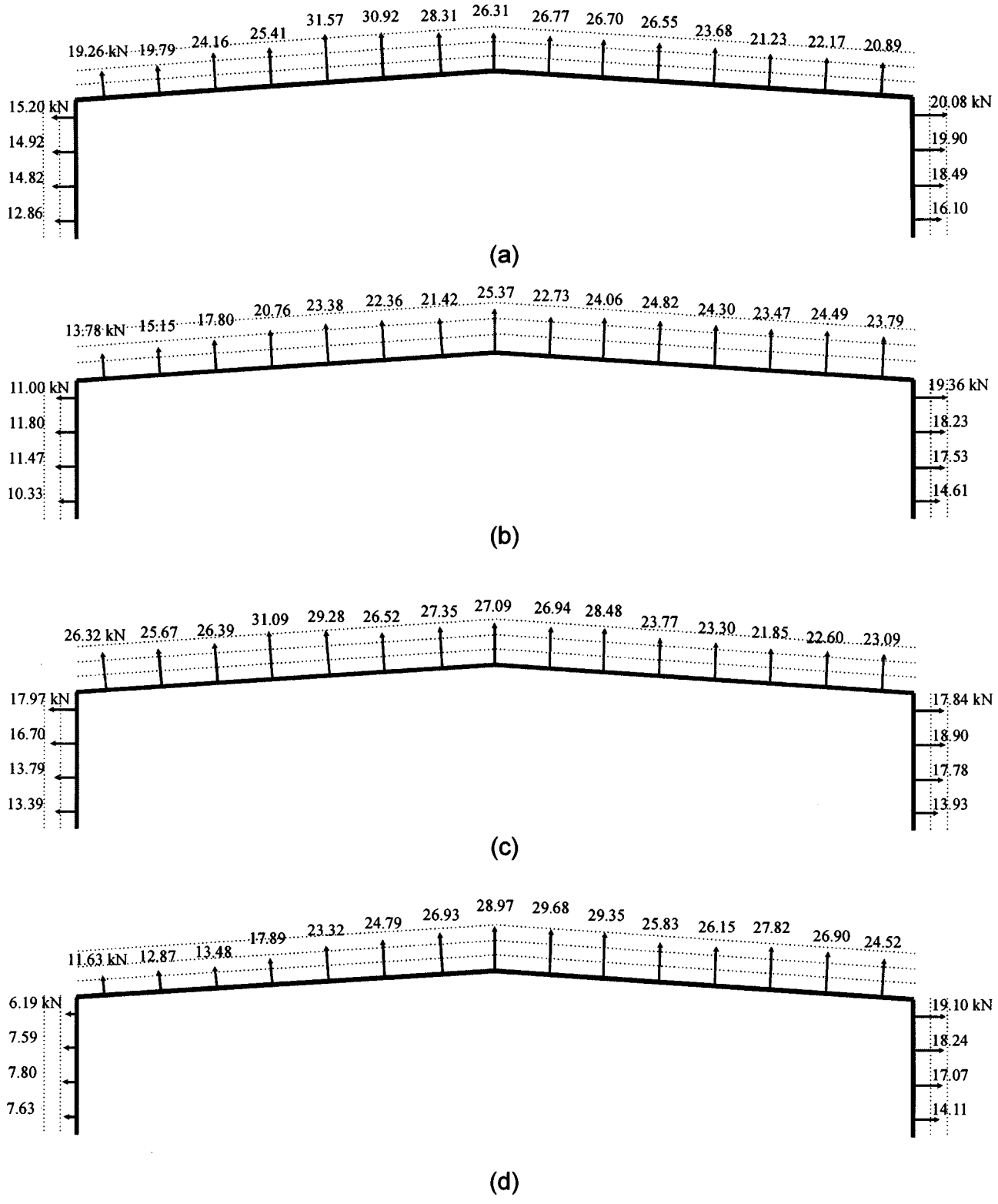

Fig. 5. Wind forces W_T acting on frame 4, wind direction (a) 0°, (b) 5°, (c) 10°, (d) 20°

load based on the wind tunnel aerodynamic database described earlier) is the load that induces the largest knee-joint bending moment during the approximately 1 h prototype period of record. Fig. 4 shows that, overall, W_T is considerably smaller than the load W_S specified by ASCE 7-93, and somewhat smaller than the load specified by ASCE 7-98. It can, therefore, be expected that for this frame, the calculated factors λ, which provide measures of the ultimate capacities of the frames, will be larger for the load combinations involving W_T than for their counterparts involving W_S.

Fig. 5 shows examples of wind loads W_T inducing critical knee-joint bending moments in Frame 4 for wind directions 0, 5, 10, and 20°. It is seen that in all these instances the wind loads W_T are less severe than the loads W_S. The results presented

J. Struct. Eng. 2002.128:1594-1603.

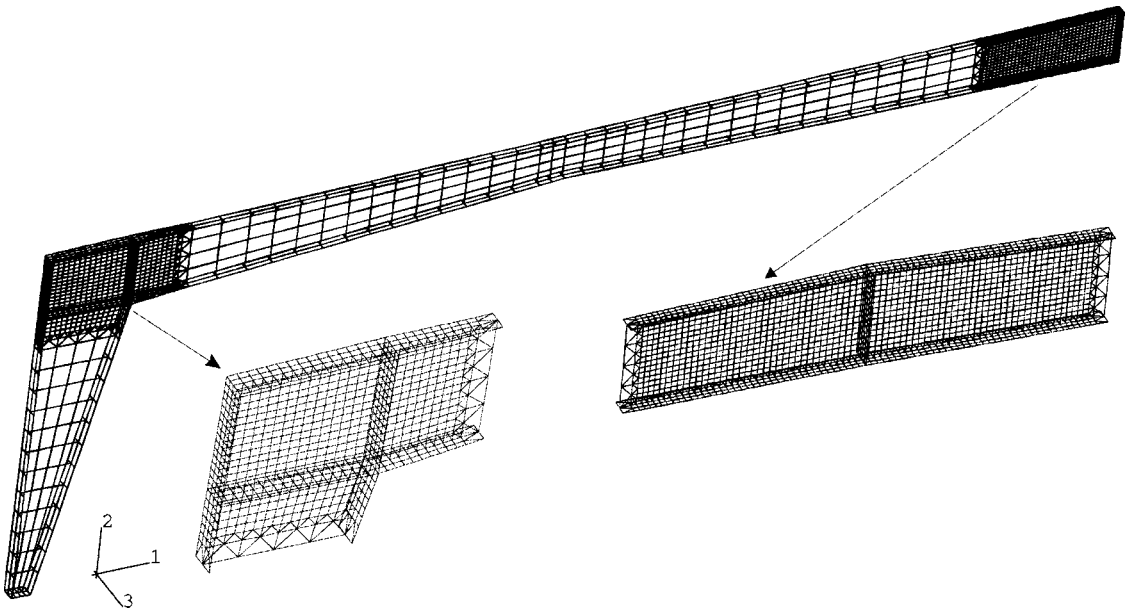

Fig. 6. Finite-element mesh of frame

in the next sections reflect this fact. The asymmetry of the loads for the 0° wind direction is due to the stochastic nature of the pressures. Although statistics of the pressures at symmetric locations are the same, the instantaneous pressures are not.

Finite Element Analyses

Finite Element Model

The general-purpose finite element analysis program ABAQUS (ABAQUS 1998) was used to perform the ultimate strength analysis of the whole frame. For most finite element analyses, the results are sensitive to the types of elements as well as the mesh density and orientation used in the model. A convergence study, thus, was performed not only for selecting a suitable shell element, but also for judging what level of mesh refinement produces a suitable mesh to give acceptable results for the frame model. The study included six types of shell elements combined with five levels of mesh generation: S4R and S3R, general-purpose shell elements, and S4R5, S8R5, S9R5, and STRI65, thin shell elements (see ABAQUS 1998 for the characterization of these elements). Triangular shell elements, S3R and STRI65, were used only for transitions from coarse to fine mesh that avoid abrupt size changes, and were combined with four-node shell elements (S4R, S4R5) and eight- or nine-node shell element (S8R5, S9R5), respectively. Convergence was studied through an examination of the deformation and stress distribution at some highly stressed regions of the structure (near the knee joints and ridge). The doubly curved general-purpose shell elements (S4R and S3R) give robust and accurate solutions in most applications and allow transverse shear deformation (accounting for finite membrane strains as well as allowing changing in plate thickness due to loading), and are suitable for large-strain analysis involving materials with a nonzero effective Poisson's ratio. On the other hand, the thin shell elements (S4R5, S8R5, S9R5, and STRI65) have some limitations, i.e., they cannot be used for cases where transverse shear deformation is not negligible. S8R5 and S9R5 require extensive computation time when fine meshes are used. The general-purpose shell elements, S4R and S3R (four-node doubly curved and three-node triangular elements with reduced integration), with very fine meshes generally showed accurate results throughout the study and were therefore selected for the ultimate strength analysis (Fig. 6).

The mesh had a total of approximately 4,600 shell elements and 4,700 nodes, resulting in approximately 28,200 degrees of freedoms. The areas of interest in the ultimate strength analysis are primarily near the knee joints and the ridge where undesirably high stresses occur, possibly producing plastic deformations. The finite element model for the frame was thus designed with locally refined mesh at both the knee joints and the ridge (using about 60% of the total mesh sizes). The aspect ratio of the elements was about 1:1–1:2 for the web plates and 1:1–1:4 for the flange plates of the frame. All the frame models were analyzed under pin-ended conditions at the center of the base of both columns. This is consistent with the boundary condition assumed in the MBMA design. Grade 50 steel [345 MPa (50 ksi) of nominal yield stress and 448 MPa (65 ksi) of nominal ultimate tensile strength] was assumed for all the columns and rafters. The modulus of elasticity, E, is 200 GPa (29,000 ksi), while the nominal tensile and nominal maximum strains are 0.15 and 0.35, respectively. An idealized trilinear elasto-plastic material behavior was assumed for the stress–strain relationship. The three lines identifying the nominal stress-strain curve intersect each other at the yield stress and strain; and at the tensile stress and strain, with the third portion extending horizontally to the maximum strain. The nominal stress–strain curve was adjusted to establish the true stress-true plastic strain curve to be used in ABAQUS using the following conversions:

$$\sigma_{\text{true}} = \sigma_{\text{nom}}(1 + \varepsilon_{\text{nom}}) \tag{4}$$

$$\varepsilon_{\text{true}} = \ln(1 + \varepsilon_{\text{nom}}) \tag{5}$$

$$\varepsilon_{\text{pl}} = \varepsilon_t - \sigma_{\text{true}}/E \tag{6}$$

In the above equations, σ_{true} and σ_{nom}=true and nominal stress, respectively, while $\varepsilon_{\text{true}}$, ε_{nom}, ε_{pl}, and ε_t=true, nominal, plastic, and total true strain, respectively.

J. Struct. Eng. 2002.128:1594-1603.

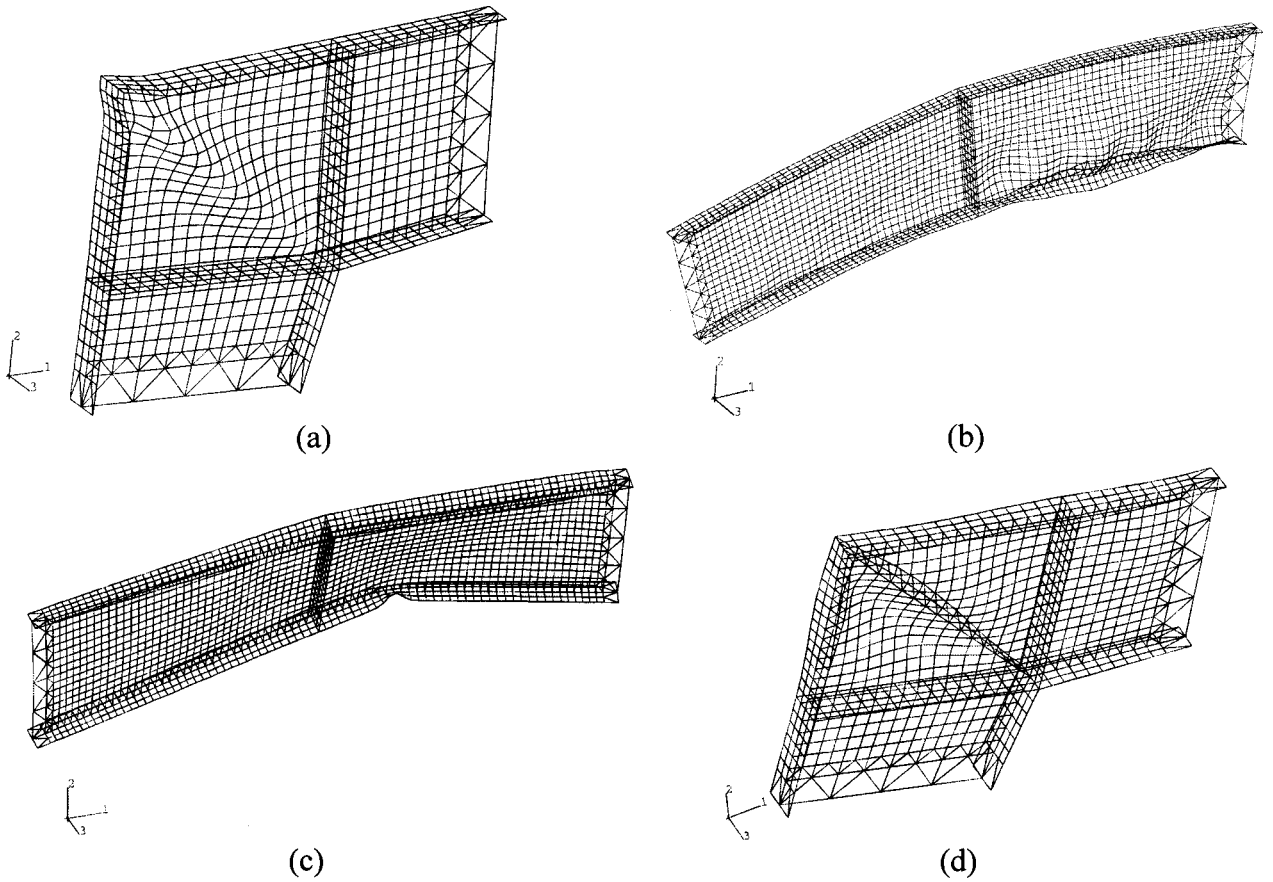

Fig. 7. Dominant failure modes and locations of instabilities, (a) web plate and outer flange local instability (MBH5, $\phi=20°$), (b) web plate and compression flange local instability (MBD5, $\phi=20°$), (c) lateral-torsional instability (RMBD5, $\phi=20°$), (d) web plate and outer flange local instability (RMBD5, $\phi=20°$)

Ultimate Strength Analyses

The study was carried out using two types of analysis. The first was an eigenvalue buckling analysis. The behavior of a real structure component is usually very different from that of the corresponding idealized component, and the reason is often the presence of initial imperfections in the real structure. Unless the precise shape of the geometric imperfections is known, a suitable imperfection based on a properly selected buckling mode needs to be specified. The eigenvalue analysis was first performed to investigate the imperfection sensitivity of the calculated strength of the frame. Through a careful examination of the first to twentieth buckling modes, the mode that gave consistently the most conservative results was selected and used in the second analysis. The selected mode defines the pattern of the initial out of flatness of the plate elements and the initial out of straightness (or crookedness) of the columns and rafters of the frame. The maximum out-of-flatness value assumed was 4.2 mm (approximately equal to the thickness of the thinnest web plate) for the web plate near the ridge. The maximum out of straightness assumed for the rafter was 6.4 mm. These values are in line with the fabrication tolerance set by the construction industry (ANSI/AWS 1996). The second type of analysis, which is the ''ultimate strength analysis,'' provides the full range prediction of the load-deformation behavior of the structure, including nonlinear material properties and changes of geometry. The Rik's method (see ABAQUS 1998) can be used in the nonlinear analysis with force or displacement control. The force control is used in the Rik's method for cases where the loading is proportional—that is, where the load magnitudes are governed by a single scalar parameter. This method can provide a solution even in cases of complex, unstable response, and can be useful for solving ill-conditioned problems such as limit state problems or almost unstable problems that exhibit softening. The second analysis, therefore, used the Rik's method with force control and was performed not only to study such effects as yielding and local instability, but also to determine the ultimate strength of the frame as a whole.

All the frames failed by instability. The results showed that the primary cause of failure of the frame MBH was web plate and compression flange local instability in the windward knee joint [Fig. 7(a)]. Frame MBD generally failed with web plate and compression flange local instability occurring in the rafter close to the ridge [Fig. 7(b)]. On the other hand, frame RMBD generally experienced somewhat excessive rotation and out-of-plane deformation of the rafter close to the ridge before failure [Fig. 7(c)]. This caused a secondary local instability at the windward knee joint [Fig. 7(d)]. Failure modes occurring in the vicinity of the ridge suggest the need to consider loadings corresponding to times at which peak moments occur at cross sections other than the knee (e.g., ridge or rafter quarter span). In this study, it was found that considering these loadings did not alter significantly the results reported herein. For other types of frame configurations, this may not be the case. Therefore, it is suggested that the extent to which such loadings may yield significant information be further studied.

J. Struct. Eng. 2002.128:1594-1603.

Table 1. Maximum Moment at Knee Joint Due to Wind Loads Based on Wind Tunnel Data

Frame	Frame 1 (Center)		Frame 2		Frame 3		Frame 4 (Outer)		
Wind direction (degrees)	Max moment [kN/m]	Time (K) [$K=1/400$ s]	Max moment [kN m]	Time (K) [$K=1/400$ s]	Max moment [kN m]	Time (K) [$K=1/400$ s]	Max moment [kN m]	Time (K) [$K=1/400$ s]	Critical frame
0	383.90	7276	390.89	7274	420.83	2871	**879.89**	1426	Frame #4
5	364.75	14137	380.74	14136	441.86	940	**781.52**	12260	Frame #4
10	419.17	10599	411.69	10597	479.13	10600	**865.86**	16355	Frame #4
15	406.28	3335	414.90	3334	464.86	3414	**834.85**	3413	Frame #4
20	450.90	7081	454.78	7077	476.54	10039	**885.20**	20711	Frame #4
25	476.01	4201	477.70	4201	495.52	1076	**807.39**	16280	Frame #4
30	522.73	3012	535.84	3002	529.50	18594	**858.84**	1969	Frame #4
35	529.04	23800	545.71	23800	577.36	23800	**817.27**	3998	Frame #4
40	540.94	14502	564.15	14509	589.60	14503	**886.78**	16579	Frame #4
45	626.26	10957	687.50	10957	713.64	10956	**818.50**	13025	Frame #4
50	639.51	670	636.97	670	657.70	670	**760.45**	19027	Frame #4
55	698.73	22006	675.64	22006	652.23	9008	**702.93**	9008	Frame #4
60	665.66	21826	**684.70**	21826	640.21	21948	655.75	8425	Frame #2
65	770.52	7959	766.81	7959	**780.23**	7959	771.10	7959	Frame #3
70	722.71	15379	**770.26**	15379	718.36	15380	614.15	2238	Frame #2
75	691.34	4242	**696.26**	4245	631.73	4234	636.44	8704	Frame #2
80	734.84	22942	**769.40**	22942	704.02	22943	695.79	22943	Frame #2
85	**761.46**	9168	692.43	17143	677.73	9150	652.78	6492	Frame #1
90	**713.92**	1479	707.19	6489	683.33	9716	696.71	7365	Frame #1
95	687.98	21858	**710.44**	6570	695.56	6577	693.31	21426	Frame #2
100	**723.19**	2064	662.95	2065	662.86	2121	620.59	2129	Frame #1
105	720.65	11371	724.46	11371	735.83	7995	**764.04**	7995	Frame #4
110	740.84	21450	**764.05**	1217	741.49	1218	716.64	1211	Frame #2
115	663.64	17641	705.54	17641	706.58	17653	**834.90**	17654	Frame #4
120	668.94	20105	651.49	20106	616.96	20100	**702.95**	6839	Frame #4

Results

For frames 1 through 4, and for various wind directions, Table 1 shows the peak knee-joint bending moments induced in the linear structure by external wind loads W_T corresponding to wind directions 0 to 120° at 5° intervals due to the 50 year wind speed specified in the ASCE 7-93 Standard (1993). These moments include the effect of the time-invariant internal pressures. Also shown in Table 1 are the instants in time at which those peak values occurred, in nondimensional units K. The total length of the wind tunnel record (corresponding to a prototype time of about 1 h) is $K_{\max}\cdot t_1=59.78$ s, where $t_1=1/400$ s is the time step of the wind tunnel time series; and the largest value of the nondimensional time parameter K is $K_{\max}=23{,}912$. The numbers in bold type indicate the critical frame, that is the frame with the largest knee-joint bending moment for each wind direction. For example, for the 85° direction, the frame experiencing the largest knee-joint moment of all internal frames is Frame 1.

Note that the wind pressure values given in Fig. 4(b) are for Frame 1, with a wind direction of 90°. For Frame 1 the largest moment occurs for 85°. Owing to symmetry, one would expect the moment for direction 95° to have the same value. However, due to sampling errors (the time histories for those directions may be viewed as different samples of the same stochastic process) the difference between the respective peak moments is quite substantial. Future research and standard development efforts may need to take such sampling errors into account.

Table 2 shows the values of the factors λ defining the ultimate

Table 2. Ultimate Strengths, λ, for MBH, MBD, and RMBD for Seven Selected Load Cases, Frame 1.

Frame model	Load case 1 $\lambda(D+L_R)$	Load case 2[a] $\lambda(D+W_S)$	Load case 3 $\lambda(D+W_T)$	Load case 4[a] $1.2D+\lambda W_S+0.5L_R$	Load case 5 $1.2D+\lambda W_T+0.5L_R$	Load case 6[a] $0.9D+\lambda W_S$	Load case 7 $0.9D+\lambda W_T$
MBH	1.700	1.639 (1.966)	2.345	1.379 (1.480)	1.616	1.449 (1.692)	2.081
MBD	1.712	1.647 (1.978)	2.382	1.392 (1.548)	1.812	1.479 (1.699)	2.157
RMBD	1.120	1.383 (1.799)	2.771	1.200 (1.439)	1.696	1.247 (1.570)	1.901

[a]Under load cases 2, 4, and 6; numbers not in parentheses and between parentheses are ultimate strengths estimated based on ASCE 7-93 and ASCE 7-98 provisions, respectively.

J. Struct. Eng. 2002.128:1594-1603.

Table 3. Ultimate Strengths, λ, for Various Wind Directions (Load Cases 5 and 7)

Wind direction (degrees)	Load Case 5 $1.2D+\lambda W_T+0.5L_R$			Load Case 7 $0.9D+\lambda W_T$			
	MBH5	MBD5	RMBD5	MBH7	MBD7	RMBD7	Critical frame
0	1.466	1.470	1.363	1.602	1.628	1.469	Frame #4
5	1.574	1.618	1.483	1.719	1.770	1.640	Frame #4
10	1.448	1.468	1.423	1.585	1.627	1.504	Frame #4
20	1.277	1.402	1.314	1.324	1.490	1.373	Frame #4
30	1.307	1.478	1.381	1.410	1.617	1.475	Frame #4
40	1.414	1.474	1.333	1.533	1.582	1.428	Frame #4
45	1.399	1.463	1.405	1.515	1.521	1.505	Frame #4
50	1.557	1.561	1.534	1.736	1.800	1.629	Frame #4
60	1.832	1.853	1.688	2.191	2.248	1.927	Frame #2
70	1.653	1.671	1.553	1.889	1.892	1.717	Frame #2
80	1.704	1.783	1.618	1.970	2.065	1.796	Frame #2
85	1.740	1.780	1.525	1.869	1.929	1.697	Frame #1
90	1.616	1.812	1.485	2.081	2.157	1.901	Frame #1
100	1.756	1.796	1.634	2.069	2.082	1.860	Frame #1
110	1.695	1.715	1.540	1.899	1.932	1.723	Frame #2
115	1.563	1.571	1.414	1.697	1.702	1.543	Frame #4
120	1.756	1.760	1.613	2.011	2.043	1.812	Frame #4
		Load case 4 $1.2D+\lambda W_S+0.5L_R$			Load case 6 $0.9D+\lambda W_S$		
All directions[a]	1.379	1.392	1.200	1.449	1.479	1.247	All Frames
All directions[b]	1.480	1.548	1.439	1.692	1.699	1.570	Frame #1∼3
	1.421	1.490	1.384	1.591	1.615	1.495	Frame #4

[a]Ultimate strengths of frames using wind loading obtained from ASCE 7-93.

[b]Ultimate strengths of frames using wind loading obtained from ASCE 7-98.

capacities of the frame for the seven load combinations listed. A main purpose of this paper is to compare the values of that factor for the load combinations in which the wind load based on the aerodynamic database, W_T, is used, and their counterparts using the ASCE 7-93 Standard (1993) and ASCE 7-98 Standard (1998) wind loadings, W_S. This comparison can be made on the basis of the results shown in Table 2, which pertains to Frame 1, direction 90°. For this frame, it is seen that in all loading cases the ASCE 7-93 wind load results in λ values that are considerably lower than those inherent in the more realistic wind loading obtained directly from the wind tunnel information. Table 2 also shows that the addition of diagonal stiffeners to the knee joint has a small effect on the ultimate capacity of the frame. By providing lateral bracing for the rafters' lower flanges at about 2.5 m distances instead of about 6 m distances, the ultimate capacity is increased by about 5–20%. The ASCE 7-98 loads are seen to represent in some instances an improvement over the ASCE 7-93 loads.

Table 3 lists calculated values of λ for load cases 5 and 7 and the critical frames corresponding to wind directions 0 to 120°. Values of λ corresponding to the ASCE 7-93 and ASCE 7-98 loads are also presented. Table 3 shows that in most cases the loads specified by the ASCE 7-93 Standard are very conservative, especially for Frames 1 and 2. The conservatism is reduced in the case of ASCE 7-98 loads. On the other hand, for MBH Frame 4, for directions 20° and 30°, the λ factors computed by using W_S are smaller than those computed by using W_T. It was verified that in this and similar cases, the spatial configuration for the load involving W_T is such that it induces moments, at cross-sections near the ridge and quarter-points of the rafter, that in some instances are larger than those induced by the ASCE 7 loads. Thus, for this frame the ASCE 7 loads can be unconservative. These observations illustrate the inconsistency with respect to risk inherent in the ASCE 7 wind loads.

From those observations it is concluded that a modest strengthening of those cross sections with respect to the ASCE-based designs would increase the safety of the structure. On the other hand, the amount of material can be reduced for most other cross sections and frames, without detriment to the safety of the structure, and with significant advantage from an economy viewpoint. Such modified designs for various frames are believed to be fully consistent with current fabrication technologies that allow differentiated frame designs at modest additional costs.

It is noted that considerations of load redistribution among frames would not significantly affect these conclusions, since ultimate capacities in various frames are not induced simultaneously, but rather by extreme winds blowing from different directions. For example, for Frame 1 the critical wind direction is normal or nearly normal to the ridge, while for Frame 4 it is parallel or nearly parallel to the ridge.

It is also noted that, while the ASCE 7 wind loads are affected by a directionality reduction factor of 0.85, the loads obtained from the aerodynamic database were not subjected to any reduction for directionality effects. Recent studies of directionality effects on frames suggest that, for loads with long mean recurrence intervals and buildings whose orientation is not known at the design stage, a directionality reduction factor of about 0.9 to 0.95 (rather than 0.85) is appropriate (Rigato, Chang, and Simiu 2001). Therefore, the factors λ should actually be somewhat larger than reported in this paper for the database-assisted estimates, and

J. Struct. Eng. 2002.128:1594-1603.

somewhat smaller for the ASCE 7-93-based estimates. This strengthens the conclusion that database-assisted design can lead to structures that are both significantly safer *and* more economical.

Conclusions

The results show that inherent in the ASCE 7 Standard wind loads are inconsistencies with respect to risk that can be significantly reduced by using database-assisted design procedures (see, e.g., Whalen et al. 2000). Such procedures are capable of producing designs that are significantly safer and more economical than designs based on the provisions of the ASCE 7's analytical method. This can be attributed to the following factors. First, inherent in the ASCE 7 provisions are simplifications due to the difficulty of reproducing the complicated spatial variation of the wind loads. Second, the ASCE 7 Standard wind loads on low-rise buildings are based on wind tunnel measurements of pressures at a number of taps lower by almost one order of magnitude than the number of taps made possible by current wind tunnel measurement technology. The representation of the wind loads would therefore be considerably cruder in the ASCE 7 provisions even if the latter did not resort to the simplifications pertaining to the spatial structure of the wind loads. We note that the loads in the ASCE 7-98 Standard are an improvement over the ASCE 7-93 loads. However, even in this case, risk consistency can be substantially improved.

The conclusions are based on the assumption that the most unfavorable wind load occurs at the time at which the peak moment is attained at the critical knee joint, and that it is equal to that load throughout the duration of the storm. This assumption was verified for a large number of cases. Failure modes observed in the vicinity of the ridge, however, suggest the need to consider loadings corresponding to times at which peak moments occur at cross sections other than the knee (e.g., ridge or rafter quarter span). In this study, it was found that considering these loadings did not alter significantly the results reported herein. For other types of frame configurations, this may not be the case. Therefore, it is suggested that the extent to which such loadings may yield significant information be further studied.

We did not address in our paper the issue of sampling errors due to the dependence of the wind loading on the realization of the loading process. Valuable contributions have been reported by J. D. Holmes in Australia and M. Kasperski in Germany. The approach we intend to take is one based on simulations of the spatio-temporal pressure field, which will allow repeating the calculations described in this paper a sufficient number of times. We intend to use database-assisted design software (Whalen et al. 2000) to provide input to the ABAQUS program in a user-friendly, effective manner.

Acknowledgments

The writers acknowledge with thanks partial support for S. Jang and L.-W. Lu by the NIST/Texas Tech University Cooperative Program Agreement/Windstorm Mitigation Initiative, and for F. Sadek and E. Simiu by the Metal Building Manufacturers Association. The work of G. Harris of CECO Building Systems, who performed the design of the building studied in this paper, is also acknowledged with thanks. Certain trade names or company products are mentioned in the text to specify adequately the procedure used. In no case does such identification imply recommendation or endorsement by NIST, nor does it imply that the product is the best available for the purpose.

References

ABAQUS. (1998). *ABAQUS/Standard, User's Manual*, Hibbitt, Karlsson and Sorensen, Inc., Providence, R.I.

ANSI/AWS. (1996). ''Structural welding code for steel.'' *ANSI/AWS D1.1-96*, American Welding Society, Miami.

ASCE Standard 7-93. (1993). ''Minimum design loads for buildings and other structures.'' Structural Engineering Institute, American Society of Civil Engineers, Reston, Va.

ASCE Standard 7-98. (1998). ''Minimum design loads for buildings and other structures.'' Structural Engineering Institute, American Society of Civil Engineers, Reston, Va.

Davenport, A. G., Surry, D., and Stathopoulos, T. (1977). ''Wind loads on low rise buildings, Part 2, Appendices.'' Boundary Layer Wind Tunnel Laboratory, Univ. of Western Ontario, London, Ontario, Canada.

Ellingwood, B. R., Galambos, T., McGregor, J., and Cornell, C. A. (1980). ''Development of a probability based load criterion for American National Standards A58.'' *NBS Special Publication 577*, National Bureau of Standards, Washington, D.C., 115.

Lin, J., and Surry, D. (1997). ''Simultaneous time series of pressures on the envelope of two large low-rise buildings.'' *BLWT-SS7-1997*, Boundary Layer Wind Tunnel Laboratory, Univ. of Western Ontario, London, Ontario, Canada.

Minciarelli, F., Gioffrè, M., Grigoriu, M., and Simiu, E. (2001a). ''Estimates of extreme wind effects and wind load factors: Influence of knowledge uncertainties.'' *Probab. Eng. Mech.*, 16, 331–340.

Minciarelli, F., Sadek, F., Simiu, E., and Grigoriu, M. (2001b). ''Structural reliability estimates and database-assisted design for wind.'' *Proc., Int. Conf. on Structural Safety and Reliability (ICOSSAR)*, R. Corotis and G. I. Schueller, eds., Newport Beach, Calif.

Rigato, A., Chang, P., and Simiu, E. (2001). ''Database-assisted design, standardization, and wind direction effects.'' *J. Transp. Eng.*, 127(8), 855–860.

Simiu, E., and Scanlan, R. H. (1996). ''*Wind effects on structures*,'' 3rd ed., Wiley, New York, 70.

Whalen, T., Shah, V., and Yang, J. S. (2000). ''A pilot project for computer-based design of low-rise buildings for wind loads—the WiLDE-LRS user's manual.'' *NIST GCR 00-802*, National Institute of Standards and Technology, Gaithersburg, Md.

Whalen, T., Simiu, E., Harris, G., Lin, L., and Surry, D. (1998). ''The use of aerodynamic databases for the effective estimation of wind effects in main wind-force resisting systems: Application to low buildings.'' *J. Wind. Eng. Ind. Aerodyn.*, 77 and 78, 685–693.

J. Struct. Eng. 2002.128:1594-1603.